ACS Energy LETTERS

Cite This: ACS Energy Lett. 2019, 4, 2632−2638

http://pubs.acs.org/journal/aelccp

LETTER

Guidelines for Optimizing the Performance of Metal−Insulator−Semiconductor (MIS) Photoelectrocatalytic Systems by Tuning the Insulator Thickness

Joseph Quinn, John Hemmerling, and Suljo Linic*

Department of Chemical Engineering, University of Michigan, Ann Arbor, Michigan 48109, United States

Catalysis Science and Technology Institute, University of Michigan, Ann Arbor, Michigan 48109, United States

Supporting Information

ABSTRACT: Layered metal−insulator−semiconductor (MIS) materials represent a promising platform for photoelectrocatalytic chemical transformations including solar water splitting. The introduction of insulators in these materials was motivated by the need to improve the stability of many inherently unstable semiconductors with desirable optical properties. Recently, it has been demonstrated that insulators, in addition to improving the stability, can also improve performance. Specifically, it was shown that the generated photovoltage of some MIS systems is highly affected by optimizing insulator thickness. In this study, we quantify the extent to which insulator tuning can be used to optimize photovoltage. This is shown experimentally by comparing the performance of two systems with inherently different barrier heights but, otherwise, identical optical and electrocatalytic properties for the hydrogen evolution reaction (HER). These photocathodes contained a p-type Si light absorber, an HfO_2 insulator, and a layered Ti−Pt or Al−Pt electrocatalyst. A comprehensive model was developed to illuminate the underlying processes governing performance and guide the design of MIS systems.

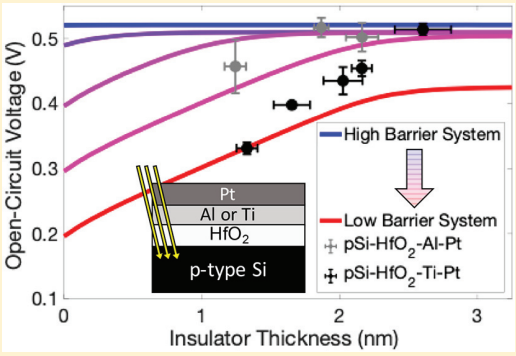

Typical photoelectrochemical water splitting systems consist of a semiconductor light absorber and a chemically attached electrocatalyst.[1,2] This system converts solar to chemical energy through a series of steps, including (1) absorption of photons by the semiconductor to form electron−hole pairs in the semiconductor, (2) migration of energetic charge carriers from the semiconductor to the electrocatalyst, and (3) the reduction and oxidation reactions induced by these charge carriers at the electrocatalytic sites. To maximize the efficiency of this overall process, various strategies have been developed to minimize energetic losses in each of these steps. For example, to maximize photon absorption, tandem (dual) semiconductors can be used to capture a larger portion of the solar spectrum compared to single absorber systems.[3,4] Recombination losses during the charge carrier migration step can be minimized by decreasing the charge carrier migration distance or by focusing light absorption at the semiconductor surface with the use of plasmonics.[5−8] Losses associated with the reduction and oxidation half-reactions can be reduced by improving the electrocatalytic activity of electrocatalysts[9−11] or maximizing the photovoltage that the semiconductor provides by reducing the parasitic recombination losses in the electrocatalyst.

For a semiconductor/electrocatalyst system to generate high photovoltage, a high interfacial built-in potential difference between a semiconductor and the attached electrocatalyst is required. This built-in potential is fundamentally governed by the inherent differences in the electronic Fermi levels between the semiconductor and metal (semiconductor Fermi level and metal work function). The built-in potential (V_{bi} in Figure 1a) creates an interfacial electric field, leading to a potential barrier (the barrier height (ϕ_{bh} in Figure 1b)) for the flow of majority carriers across the interface. Under illumination, this electric field drives energized minority carriers toward the electrocatalyst and majority carriers in the opposite direction, therefore preventing their parasitic recombination. While, in principal, the barrier height is calculated as the difference between the isolated semiconductor valence band edge and the

Received: July 26, 2019
Accepted: October 8, 2019
Published: October 8, 2019

DOI: 10.1021/acsenergylett.9b01609
ACS Energy Lett. 2019, 4, 2632−2638

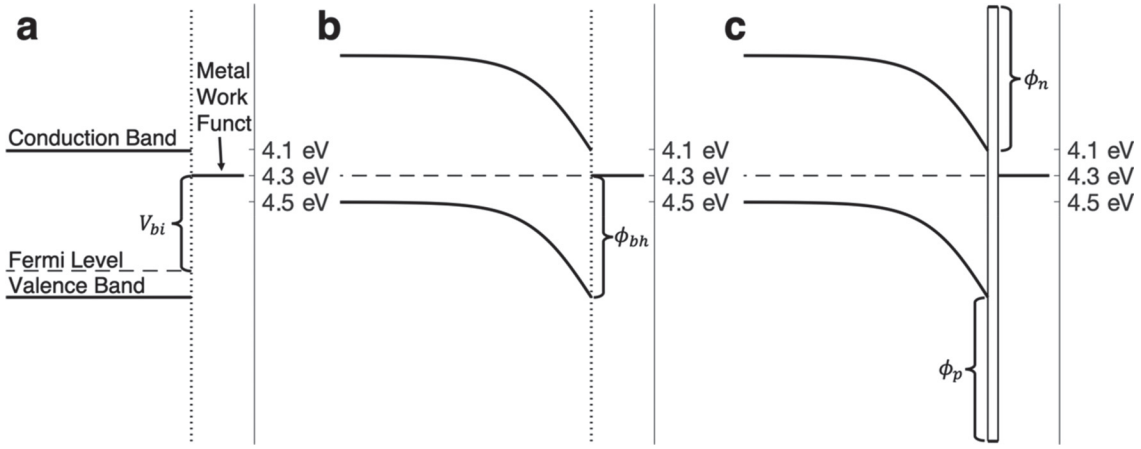

Figure 1. Semiconductor energy band diagrams. (a) Schematic of a noninteracting p-type semiconductor (silicon) and a low work function metal (4.3 eV) energy diagrams. (b) Schematic of p-type silicon coupled to the metal at equilibrium under no illumination; the potential barrier for majority carriers is called the barrier height ϕ_{bh} and is dependent on the metal work function. (c) Schematic of an equilibrated MIS interface. The insulator creates an energetic barrier for electrons and holes (ϕ_n and ϕ_p).

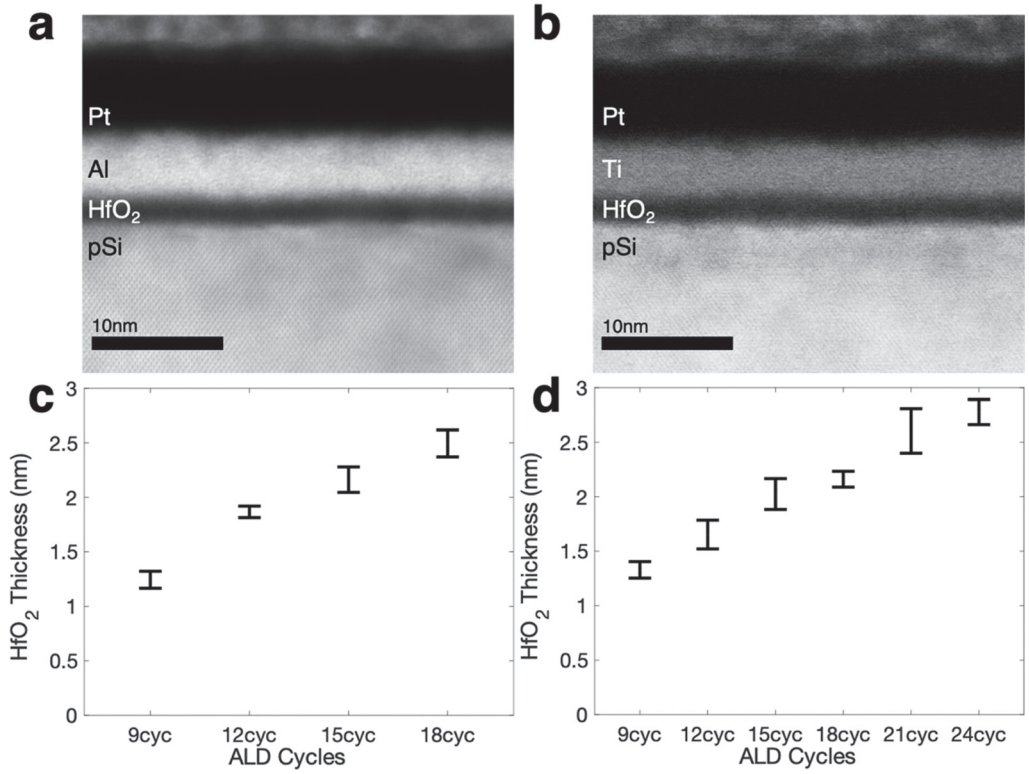

Figure 2. STEM cross-sectional micrographs and insulator thicknesses of the photocathode systems. (a) STEM cross section of the pSi-HfO_2−Al−Pt sample with 15 ALD cycles. (b) STEM cross section of the pSi-HfO_2−Ti−Pt sample with 15 ALD cycles. (c) Insulator thickness-to-ALD cycle relationship for the pSi-HfO_2−Al−Pt samples. (d) Insulator thickness-to-ALD cycle relationship for the pSi-HfO_2−Ti−Pt samples.

metal Fermi level, various studies have shown that the presence of surface states at the interface causes experimentally measured barrier heights to be significantly lower, thus diminishing generated photovoltage.[12,13] Additionally, many semiconductor−electrocatalyst pairs suffer from an inherently low difference in the respective Fermi level positions and therefore form low barrier heights.

There are multiple approaches proposed to address the problem of a poor barrier height between an electrocatalyst and semiconductor. Methods include the fabrication of a p−n junction within the semiconductor beneath the electrocatalyst layer, which generates large electric fields in the semiconductor that force the separation of charge carriers.[14−21] Another approach is to introduce two metal layers at the semiconductor electrocatalyst junction. In this system, the inner metal layer that is in direct contact with a semiconductor sets the interfacial built-in potential and has the desired work function, while the outer layer serves as an active electrocatalyst.[22−25]

DOI: 10.1021/acsenergylett.9b01609
ACS Energy Lett. 2019, 4, 2632−2638

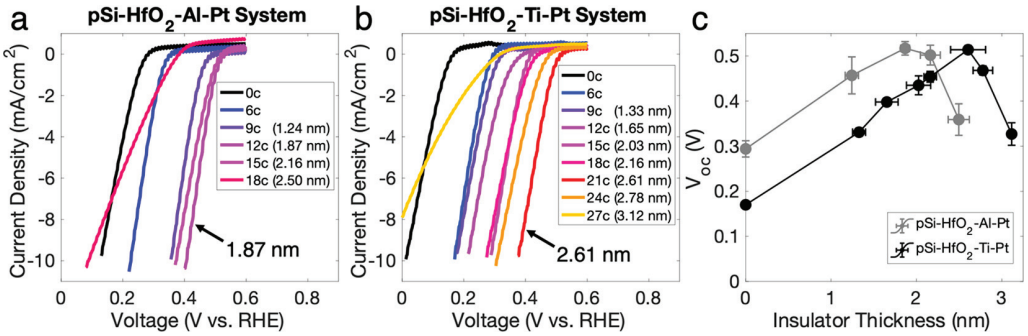

Figure 3. Electrochemical performance of the photocathodes in light-driven HER. (a,b) Linear sweep voltammograms of the pSi-HfO_2−Al−Pt and pSi-HfO_2−Ti−Pt electrodes at various insulator thicknesses. (a) The photovoltage of the pSi-HfO_2−Al−Pt samples improves with insulator thickness up to 1.9 nm and decreases thereafter. The photovoltage for the highest-performing insulator thickness is 517 mV. (b) The pSi-HfO_2−Ti−Pt samples show improving photovoltage up to 2.6 nm, after which it decreases. The photovoltage for the highest-performing insulator thickness is 514 mV. (c) V_{oc} for the pSi-HfO_2−Al−Pt and pSi-HfO_2−Ti−Pt samples plotted as a function of increasing insulator thickness.

We have recently demonstrated another strategy to address the problem of a poor barrier height in order to generate a high photovoltage for a variety of semiconductors.[26] This approach involves the use of a metal(electrocatalyst)−insulator−semiconductor (MIS) system, which had previously been used in a variety of recent photoelectrochemical studies.[27−34] In this approach, the insulator—we focused on insulators that conduct charge via a tunneling mechanism—changes the semiconductor band energetics by creating an additional barrier for both electrons and holes, as shown in Figure 1c. We showed that in these systems by tuning the thickness of the insulator layer it was possible to control the flux of charge carriers from the semiconductor to the electrocatalyst and by doing so minimize the recombination losses and optimize the generated photovoltage, i.e., the insulator improved the photovoltage of the system that had an inherently poor semiconductor/electrocatalyst barrier height by reducing recombination. We note that the insulators in these systems are also employed to protect the semiconductor from the corrosive electrolyte environment.[17,32,34−44]

In this contribution, we attempt to quantify the extent to which tuning the insulator thickness can improve photovoltage. Specifically, we investigate if tuning the insulator thickness enables a system with an inherently poor barrier height to perform as well as a system with a better inherent barrier height. We perform our analysis by way of a concrete example of the H_2 evolution reaction (HER) on an illuminated p-type silicon (pSi) semiconductor covered with thin layers of the HfO_2 insulator and an additional metal bilayer (Al−Pt and Ti−Pt). In these systems, HfO_2 acts as a tunnel insulator, Al and Ti are metals with different work functions that control the inherent interfacial barrier height, while Pt is an excellent HER electrocatalyst. We show that by modulating the insulator thickness we are able to achieve a photovoltage of 514 mV for Ti−Pt and 517 for the Al−Pt samples, which is among the highest reported for pSi.[14] Insulator tuning was critical to enable the performance of the poor barrier system (pSi-HfO_2−Ti−Pt) to approach that of the higher barrier system (pSi-HfO_2−Al−Pt). We support the underlying physical mechanisms by a comprehensive mathematical model, which also allowed us to make a number of general conclusions that quantify the expected impact of insulator thickness on the performance of the MIS photoelectrocatalysts.

Our experimental systems consisted of pSi covered with an HfO_2 insulator layer of varying thickness. The HfO_2 was deposited with atomic layer deposition (ALD), and the thickness was varied by modifying the number of ALD cycles. We reiterate that the HfO_2 insulator transports charge between the semiconductor and electrocatalyst via a tunneling mechanism.[45,46] The HfO_2-coated pSi was covered with two metal layers. In one system, we used Al and Pt, and in the other system, we used Ti and Pt. On the basis of the tabulated work function values, Al (work function of ∼4.06−4.26 eV[47]) is expected to form a higher barrier with pSi compared to that with Ti (work function of ∼4.33 eV[48]). Each individual metal (5 nm in thickness) was deposited using e-beam evaporation.

To characterize the fabricated materials, we performed scanning transmission electron microscopy (STEM) on cross sections of the pSi-HfO_2−Al−Pt and pSi-HfO_2−Ti−Pt samples. Representative micrographs of pSi-HfO_2−Al−Pt and pSi-HfO_2−Ti−Pt samples are shown Figure 2a,b, respectively. The image shows well-defined layers of the pSi semiconductor, an amorphous HfO_2 insulator, and metal bilayers. Additional microscopic characterization is provided in the Supporting Information. By taking cross sections of additional samples, the relationship between the insulator thickness and the number of ALD cycles can be characterized. For each metal bilayer system, all imaged and experimentally tested samples with the same insulator thickness originate from the same pSi wafer. This data is presented in Figure 2c,d for the pSi-HfO_2−Al−Pt and pSi-HfO_2−Ti−Pt samples, respectively; the error bars account for thickness variation within the imaged samples.

The pSi-HfO_2−Ti−Pt and pSi-HfO_2−Al−Pt electrodes were tested in photoelectrochemical HER to determine the effect of the HfO_2 insulator thickness on the generated photovoltage. A three-electrode cell was used with a Pt wire counter electrode and an $Hg/HgSO_4$ reference electrode. The electrolyte consisted of 1 M perchloric acid with H_2 bubbling into the electrolyte throughout the experiments. The electrodes were illuminated with a halogen lamp at an intensity of 100 mW/cm^2 (∼1 sun). We define generated photovoltage as the difference in the open-circuit potential "V_{oc}" (the point where the current density crosses zero) between a working photocathode and 0 V vs RHE (corroborated by measuring the hydrogen evolution potential for a Pt wire). Additional photoelectrochemical details are provided in the Supporting Information.

DOI: 10.1021/acsenergylett.9b01609
ACS Energy Lett. 2019, 4, 2632−2638

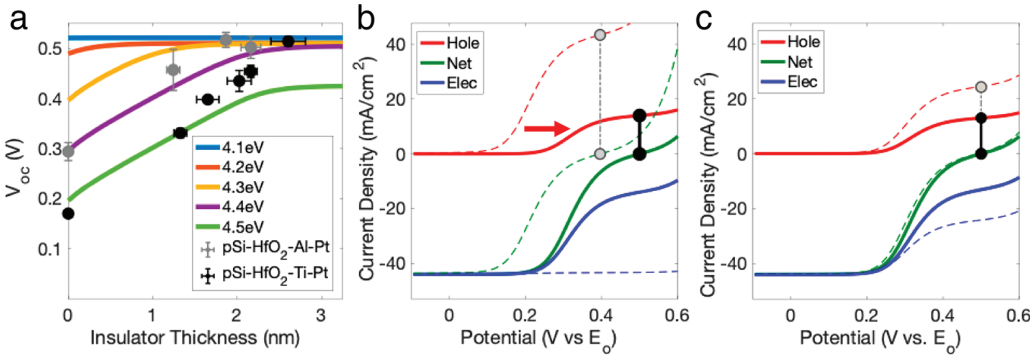

Figure 4. Modeled open-circuit voltage (V_{oc}) and charge carrier flux diagrams for a pSi-HfO_2−metal system. (a) Modeled V_{oc} as a function of insulator thickness for MIS systems with various effective metal work functions. The experimental results of the pSi-HfO_2−Al−Pt and pSi-HfO_2−Ti−Pt electrodes are also provided for comparison. (b,c) Individual charge carrier fluxes for (b) a low barrier (high effective metal work function of 4.3 eV) and (c) a high barrier (low effective metal work function of 4.2 eV). The red, green, and blue lines represent hole, net, and electron currents, respectively. The dashed lines are calculated for a zero-thickness insulator, while the solid lines represent an insulator thickness that provides a near-optimum V_{oc} of 500 mV. For (b), a 1.3 nm insulator raises V_{oc} from 400 to 500 mV. For (c), an insulator of 0.26 nm raises V_{oc} from 490 to 500 mV. The applied voltage is referenced vs the solution redox potential, E_o. The gray and black vertical lines indicate majority carrier currents at V_{oc} for the zero-thickness and optimized cases, respectively, which lead directly to recombination.

In Figure 3, we show linear sweep voltammograms generated by the two photoelectrocatalyst systems for various HfO_2 thicknesses. The data in Figure 3 show that for systems that do not contain the HfO_2 insulator the Al-containing sample achieves a higher V_{oc} (285 mV) and therefore a higher photovoltage compared to the Ti-containing sample (167 mV). While both of these samples likely suffer from a high degree of Fermi level pinning associated with a direct metal−silicon contact, the larger photovoltage generated by the pSi-Al samples implies that they have a higher inherent barrier height compared to the pSi-Ti samples. This result is not unexpected considering that Al has an inherently lower work function than Ti by ∼70−270 meV.[47,48] The difference in the barrier heights between the pSi-HfO_2−Al−Pt and pSi-HfO_2−Ti−Pt systems was corroborated by a series of Mott−Schottky experiments described in the Supporting Information, where the median barrier height for the Al-containing samples was ∼100 meV higher than that for the Ti-containing samples.

The data in Figure 3 also show that the presence of thin HfO_2 insulator layers improves the performance of both photoelectrocatalysts dramatically. For the pSi-HfO_2−Al−Pt electrodes, V_{oc} improves with an increasing HfO_2 insulator thickness from 0 to 1.9 nm to a maximum of 517 mV. After this point, increasing insulator thickness decreases the generated photovoltage. This decrease is caused by impediments to minority carrier transport due to an increasing resistance to the charge carrier tunneling. Interestingly, the data also show that the insulator thickness tuning has an even stronger effect on the pSi-HfO_2−Ti−Pt system compared to the pSi-HfO_2−Al−Pt system. In this system, the V_{oc} increases with insulator thickness up to 2.6 nm, after which it starts declining. The V_{oc} of the optimized pSi-HfO_2−Ti−Pt sample was nearly identical to that of the Al−Pt sample.

The data in Figure 3 show that, while both metal bilayer systems (Al−Pt and Ti−Pt) benefit from the insulator thickness tuning, the performance of the system with a moderate barrier (pSi-HfO_2−Ti−Pt) improves to a greater extent than the performance of the system with an inherently higher barrier (pSi-HfO_2−Al−Pt). The data show that by tuning of the insulator thickness we are able to improve the performance of a fundamentally poor barrier system so that it matches the optimized performance of the system with an inherently superior barrier height.

To further investigate the behavior of these systems, we developed, following previous contributions,[26,49] a mathematical model that can describe the underlying physical processes taking place on layered MIS photoelectrocatalysts. A detailed description of the model is provided in the Supporting Information and in the previous contributions. In short, electrochemical reaction rates on the electrocatalyst are described by the Butler−Volmer equation. This determines the electric potential required for the electrocatalyst (in this case, the top layer of Pt) to reach a specific current. The model captures the interaction of light with a semiconductor by solving Poisson's equation (which governs the semiconductor electrostatics) and charge carrier continuity equations for both charge carriers (electrons and holes). The charge carrier continuity equations track the flux of charge carriers throughout the semiconductor by capturing the absorption, recombination, and diffusion processes in the semiconductor. The boundary condition for the flux of charge carriers between the semiconductor and electrocatalyst is described using the following equations[26,49−51]

$$J_p = k_p(p_s - \overline{p}_s)\exp(-\alpha d\sqrt{\phi_p})$$
$$J_n = k_n(n_s - \overline{n}_s)\exp(-\alpha d\sqrt{\phi_n}) \quad (1)$$

In this equation, J_n and J_p are the interfacial electron and hole currents, respectively. The net current is $J_p - J_n$. k_n and k_p are the charge transfer rate coefficients for electrons and holes (these depend on the density of states in the semiconductor and metal), and we assumed the same value in this system, as is generally the case.[26,49] n_s and p_s are the electron and hole concentrations at the illuminated semiconductor surface at an applied potential, while $\overline{n}_s$ and $\overline{p}_s$ represent the surface carrier concentrations in equilibrium in the dark. The exponential terms represent the tunneling probabilities through the insulator for electrons and holes, which are dependent on a constant (α), insulator thickness (d), and the semiconductor−insulator energetic barrier for electrons and holes (ϕ_n and ϕ_p),

DOI: 10.1021/acsenergylett.9b01609
ACS Energy Lett. 2019, 4, 2632−2638

which are depicted in Figure 1c. Previous studies using HfO_2 films on silicon have shown a ϕ_n of 1.1 eV.[45] In this work, we assume a symmetric barrier, i.e., $\phi_n = \phi_p$, though the degree of symmetry is the subject of future studies. Because the solutions to Poisson's and continuity equations are interdependent, these are solved iteratively to determine the potential and charge carrier concentration profiles through the semiconductor. These profiles are useful because they can be used to calculate the current−voltage relationship (i.e., the performance) of an MIS system.

By modifying physical design parameters of the system in the model, we can determine their effect on the overall performance. The specific variables that were investigated were (1) inner metal effective work function (which adjusts the barrier height) and (2) insulator thickness. The insulator thickness (d) impacts charge carrier fluxes by exponentially decreasing the tunneling probability term (eq 1). The effective inner metal work function directly affects $\overline{n}_s$ and $\overline{p}_s$, the semiconductor (interfacial) surface carrier concentrations in equilibrium in the dark, as shown in the following equations[26,49]

$$\overline{n}_s = n_{bulk} \exp\left[\frac{-q(\phi_m - \phi_s)}{k_b T}\right]$$
$$\overline{p}_s = p_{bulk} \exp\left[\frac{q(\phi_m - \phi_s)}{k_b T}\right] \quad (2)$$

where n_{bulk} and p_{bulk} are the electron and hole concentrations in the semiconductor bulk, ϕ_m is the effective work function of the inner metal, and ϕ_s is the isolated semiconductor Fermi level. We note that eq 2 essentially captures the change in barrier height as a function of the inner metal with different work functions. We note that we use the terminology "effective work function" because, as discussed above, Schottky-based junctions often show a lower barrier height than expected (given the metal work function) due to imperfections at the interface.

To illustrate how these variables affect the performance, the dependence of increasing insulator thickness on V_{oc} was modeled for systems with different effective work functions. The data in Figure 4a show the modeled behavior of photoelectrocatalysts with inner metal effective work functions ranging from 4.1 to 4.5 eV. In the limit of a very low work function (in this case ∼4.1 eV), V_{oc} is high regardless of insulator thickness. We note that we are not addressing performance losses at higher currents, where relatively high thickness insulators lead to minority charge carrier transport resistance losses. In these systems, due to an inherently high barrier height, the open-circuit voltage cannot be improved significantly by introduction of the insulator as it is already close to the maximum V_{oc} that the semiconductor can generate. The data in Figure 4a show that systems with moderate work functions (4.2−4.4 eV) can reach the near-maximum photovoltage that the system can provide by properly tuning the insulator thickness. Finally, the data also show that for inner metals with very poor work function, 4.5+ eV, the inherently poor performance cannot be completely overcome by an introduction of insulators due to high recombination losses for any insulator thickness.

The modeling results shed light on some of the performance differences between the Al−Pt and Ti−Pt bilayer systems. The data in Figure 4a show that high barrier systems (work functions < 4.3 eV) reach a near-maximum open-circuit voltage at lower insulator thicknesses compared to moderate barrier systems (work functions > 4.3 eV). This is consistent with the experimental results, which are also shown in Figure 4a (labeled at distinct data points) for comparison, where the Al−Pt samples show optimized performance at an HfO_2 thickness of 1.9 nm while the Ti−Pt samples show optimal performance at 2.6 nm. For very thick insulators, the model cannot be applied to experimental systems, where charge carriers no longer transfer via a direct tunneling mechanism.

To determine the underlying factors that govern the relationships between the insulator thickness and V_{oc}, we studied the impact of insulator thickness on the fluxes of minority (electrons) and majority (holes) charge carriers. Figure 4b shows the charge carrier fluxes for a MIS system with a lower inherent barrier height (the inner metal work function of 4.3 eV). The dashed lines show the fluxes of individual charge carriers calculated for an unoptimized case (zero-insulator thickness), while solid lines show the fluxes for an optimized insulator thickness case (insulator thicknesses that lead to a near-maximum V_{oc} at 500 mV). The data show that for a zero-thickness insulator there are high fluxes for both charge carriers at open-circuit voltage (400 mV). The high majority carrier current is caused by a smaller electric field driving majority carriers away from the interface (i.e., $\overline{p}_s$ from eq 2 is low, resulting in a high J_p from eq 1). In this case, essentially the band bending in the semiconductor is small. The high flux of majority carriers leads to a high degree of electron−hole recombination (depicted by the gray line in Figure 4b) at V_{oc}. By introducing the insulator and tuning its thickness, the losses due to the electron−hole recombination in the electrocatalyst are minimized. This is accomplished by creating an additional barrier for the flow of charge between the semiconductor and electrocatalyst (i.e., the energetic barrier of the insulator) whose thickness allows us to tune the flow of charge carriers. The data in Figure 4c show that for this case an insulator thickness of 1.3 nm results in near-maximum photovoltage at 500 mV.

Figure 4c shows the charge carrier fluxes for a higher barrier system (low effective work function metal, 4.2 eV). For this system, the zero-insulator thickness case (dashed lines) already has very low majority carrier fluxes due to a high electric field. This leads to a high V_{oc} of 490 mV. These electrodes, with inherently desirable barrier heights, require lower insulator thicknesses (0.26 nm) to minimize majority carrier recombination and reach the maximum V_{oc} of 500 mV.

Our analyses show that insulator tuning enabled a low barrier system (pSi-HfO_2−Ti−Pt) to achieve a photovoltage of 514 mV, which was similar to the performance of a higher barrier system (pSi-HfO_2−Al−Pt) that had a photovoltage of 517 mV. The insulator thickness optimization was different for the various metal bilayer systems, with the Ti−Pt system achieving an optimized performance at 2.6 nm while the Al−Pt system had an optimized thickness at 1.9 nm. A model was developed to provide a physical description of the MIS interface. The modeling results suggest that the optimized insulator thickness and overall performance of the system are functions of the initial barrier height. The variance in insulator thickness optimization is due to differences in the level of majority carrier recombination at low insulator thickness. The low barrier systems require a thicker insulator to minimize majority carrier recombination currents compared to a higher barrier system. The work suggests that a simultaneous analysis

DOI: 10.1021/acsenergylett.9b01609
ACS Energy Lett. 2019, 4, 2632−2638

of the barrier height and insulator thickness can be leveraged to optimize performance in the design of MIS structures. These results could be particularly useful for semiconductors that have difficulties forming high barriers (e.g., high-band-gap metal oxide semiconductors that cannot form p−n junctions). These systems could implement the use of metal bilayers to create barriers as high as possible while mitigating remaining majority carrier recombination with insulator thickness optimization.

■ ASSOCIATED CONTENT

Supporting Information

The Supporting Information is available free of charge on the ACS Publications website at DOI: 10.1021/acsenergylett.9b01609.

Additional microscopic characterization, fabrication and electrochemical methods, and modeling details (PDF)

■ AUTHOR INFORMATION

Corresponding Author

*E-mail: linic@umich.edu.

ORCID

Joseph Quinn: 0000-0002-8742-7052

Suljo Linic: 0000-0003-2153-6755

Notes

The authors declare no competing financial interest.

■ ACKNOWLEDGMENTS

This work was primarily supported by the National Science Foundation (NSF) (CBET-1803991). The synthesis was developed and paid for with the support of the U.S. Department of Energy, Office of Basic Energy Science, Division of Chemical Sciences (FG-02-05ER15686). Secondary support for the development of analytical tools used in the model was provided by NSF (CBET-1702471 and CHE-1800197).

■ REFERENCES

(1) Walter, M. G.; Warren, E. L.; McKone, J. R.; Boettcher, S. W.; Mi, Q.; Santori, E. A.; Lewis, N. S. Solar Water Splitting Cells. *Chem. Rev.* **2010**, *110* (11), 6446−6473.

(2) Fan, R.; Mi, Z.; Shen, M. Silicon Based Photoelectrodes for Photoelectrochemical Water Splitting. *Opt. Express* **2019**, *27* (4), A51−A80.

(3) Seitz, L. C.; Chen, Z.; Forman, A. J.; Pinaud, B. A.; Benck, J. D.; Jaramillo, T. F. Modeling Practical Performance Limits of Photoelectrochemical Water Splitting Based on the Current State of Materials Research. *ChemSusChem* **2014**, *7* (5), 1372−1385.

(4) Chen, Y.; Hu, S.; Xiang, C.; Lewis, N. S. A Sensitivity Analysis to Assess the Relative Importance of Improvements in Electrocatalysts, Light Absorbers, and System Geometry on the Efficiency of Solar-Fuels Generators. *Energy Environ. Sci.* **2015**, *8* (3), 876−886.

(5) Hernley, P. A.; Chavez, S. A.; Quinn, J. P.; Linic, S. Engineering the Optical and Catalytic Properties of Co-Catalyst/Semiconductor Photocatalysts. *ACS Photonics* **2017**, *4* (4), 979−985.

(6) Hernley, P. A.; Linic, S. Modeling the Impact of Metallic Plasmonic Resonators on the Solar Conversion Efficiencies of Semiconductor Photoelectrodes: When Does Introducing Buried Plasmonic Nanostructures Make Sense? *J. Phys. Chem. C* **2018**, *122* (42), 24279−24286.

(7) Chavez, S.; Aslam, U.; Linic, S. Design Principles for Directing Energy and Energetic Charge Flow in Multicomponent Plasmonic Nanostructures. *ACS Energy Lett.* **2018**, *3* (7), 1590−1596.

(8) Atwater, H. A.; Polman, A. Plasmonics for Improved Photovoltaic Devices. *Nat. Mater.* **2010**, *9* (3), 205−213.

(9) Mukherjee, J.; Linic, S. First-Principles Investigations of Electrochemical Oxidation of Hydrogen at Solid Oxide Fuel Cell Operating Conditions. *J. Electrochem. Soc.* **2007**, *154* (9), B919−B924.

(10) Ingram, D. B.; Linic, S. First-Principles Analysis of the Activity of Transition and Noble Metals in the Direct Utilization of Hydrocarbon Fuels at Solid Oxide Fuel Cell Operating Conditions. *J. Electrochem. Soc.* **2009**, *156* (12), B1457−B1465.

(11) Dau, H.; Limberg, C.; Reier, T.; Risch, M.; Roggan, S.; Strasser, P. The Mechanism of Water Oxidation: From Electrolysis via Homogeneous to Biological Catalysis. *ChemCatChem* **2010**, *2* (7), 724−761.

(12) Cowley, A. M.; Sze, S. M. Surface States and Barrier Height of Metal-Semiconductor Systems. *J. Appl. Phys.* **1965**, *36* (10), 3212−3220.

(13) Rhoderick, E. H. Metal-Semiconductor Contacts. *IEE Proc., Part I: Solid-State Electron Devices* **1982**, *129* (1), 1.

(14) Hu, S.; Lewis, N. S.; Ager, J. W.; Yang, J.; McKone, J. R.; Strandwitz, N. C. Thin-Film Materials for the Protection of Semiconducting Photoelectrodes in Solar-Fuel Generators. *J. Phys. Chem. C* **2015**, *119* (43), 24201−24228.

(15) Scheuermann, A. G.; McIntyre, P. C. Atomic Layer Deposited Corrosion Protection: A Path to Stable and Efficient Photoelectrochemical Cells. *J. Phys. Chem. Lett.* **2016**, *7* (14), 2867−2878.

(16) Bae, D.; Seger, B.; Vesborg, P. C. K.; Hansen, O.; Chorkendorff, I. Strategies for Stable Water Splitting via Protected Photoelectrodes. *Chem. Soc. Rev.* **2017**, *46* (7), 1933−1954.

(17) Seger, B.; Pedersen, T.; Laursen, A. B.; Vesborg, P. C. K.; Hansen, O.; Chorkendorff, I. Using TiO2 as a Conductive Protective Layer for Photocathodic H2 Evolution. *J. Am. Chem. Soc.* **2013**, *135* (3), 1057−1064.

(18) Fan, R.; Dong, W.; Fang, L.; Zheng, F.; Shen, M. More than 10% Efficiency and One-Week Stability of Si Photocathodes for Water Splitting by Manipulating the Loading of the Pt Catalyst and TiO 2 Protective Layer. *J. Mater. Chem. A* **2017**, *5* (35), 18744−18751.

(19) Oh, S.; Oh, J. High Performance and Stability of Micropatterned Oxide-Passivated Photoanodes with Local Catalysts for Photoelectrochemical Water Splitting. *J. Phys. Chem. C* **2016**, *120* (1), 133−141.

(20) Guo, B.; Batool, A.; Xie, G.; Boddula, R.; Tian, L.; Jan, S. U.; Gong, J. R. Facile Integration between Si and Catalyst for High-Performance Photoanodes by a Multifunctional Bridging Layer. *Nano Lett.* **2018**, *18* (2), 1516−1521.

(21) Oh, S.; Song, H.; Oh, J. An Optically and Electrochemically Decoupled Monolithic Photoelectrochemical Cell for High-Performance Solar-Driven Water Splitting. *Nano Lett.* **2017**, *17* (9), 5416−5422.

(22) Digdaya, I. A.; Adhyaksa, G. W. P.; Trześniewski, B. J.; Garnett, E. C.; Smith, W. A. Interfacial Engineering of Metal-Insulator-Semiconductor Junctions for Efficient and Stable Photoelectrochemical Water Oxidation. *Nat. Commun.* **2017**, *8*, 15968.

(23) Digdaya, I. A.; Trześniewski, B. J.; Adhyaksa, G. W. P.; Garnett, E. C.; Smith, W. A. General Considerations for Improving Photovoltage in Metal−Insulator−Semiconductor Photoanodes. *J. Phys. Chem. C* **2018**, *122* (10), 5462−5471.

(24) Esposito, D. V.; Levin, I.; Moffat, T. P.; Talin, A. A. H2 Evolution at Si-Based Metal−Insulator−Semiconductor Photoelectrodes Enhanced by Inversion Channel Charge Collection and H Spillover. *Nat. Mater.* **2013**, *12* (6), 562−568.

(25) Ji, L.; McDaniel, M. D.; Wang, S.; Posadas, A. B.; Li, X.; Huang, H.; Lee, J. C.; Demkov, A. A.; Bard, A. J.; Ekerdt, J. G.; et al. A Silicon-Based Photocathode for Water Reduction with an Epitaxial $SrTiO_3$ Protection Layer and a Nanostructured Catalyst. *Nat. Nanotechnol.* **2015**, *10* (1), 84−90.

(26) Quinn, J.; Hemmerling, J.; Linic, S. Maximizing Solar Water Splitting Performance by Nanoscopic Control of the Charge Carrier Fluxes across Semiconductor−Electrocatalyst Junctions. *ACS Catal.* **2018**, *8*, 8545−8552.

DOI: 10.1021/acsenergylett.9b01609
ACS Energy Lett. 2019, 4, 2632−2638

(27) Hill, J. C.; Landers, A. T.; Switzer, J. A. An Electrodeposited Inhomogeneous Metal−Insulator−Semiconductor Junction for Efficient Photoelectrochemical Water Oxidation. *Nat. Mater.* **2015**, *14* (11), 1150−1155.
(28) Kenney, M. J.; Gong, M.; Li, Y.; Wu, J. Z.; Feng, J.; Lanza, M.; Dai, H. High-Performance Silicon Photoanodes Passivated with Ultrathin Nickel Films for Water Oxidation. *Science* **2013**, *342* (6160), 836−840.
(29) Oh, S.; Jung, S.; Lee, Y. H.; Song, J. T.; Kim, T. H.; Nandi, D. K.; Kim, S.-H.; Oh, J. Hole-Selective CoOx/SiOx/Si Heterojunctions for Photoelectrochemical Water Splitting. *ACS Catal.* **2018**, *8* (10), 9755−9764.
(30) Luo, Z.; Liu, B.; Li, H.; Chang, X.; Zhu, W.; Wang, T.; Gong, J. Multifunctional Nickel Film Protected N-Type Silicon Photoanode with High Photovoltage for Efficient and Stable Oxygen Evolution Reaction. *Small Methods* **2019**, 1900212.
(31) Park, M.-J.; Jung, J.-Y.; Shin, S.-M.; Song, J.-W.; Nam, Y.-H.; Kim, D.-H.; Lee, J.-H. Photoelectrochemical Oxygen Evolution Improved by a Thin Al2O3 Interlayer in a NiOx/n-Si Photoanode. *Thin Solid Films* **2016**, *599*, 54−58.
(32) Jung, J.-Y.; Yu, J.-Y.; Shinde, S. S.; Kim, S.-H.; Kim, D.-H.; Lin, C.; Wehrspohn, R. B.; Lee, J.-H. Remarkable Improvements in the Performance and Stability of Si Photoanodes Adopting Nanocrystalline NiOx Electrocatalyst and Stoichiometric SiO2 Protection. *Appl. Surf. Sci.* **2019**, *493*, 1150−1158.
(33) Mikolasek, M.; Frohlich, K.; Husekova, K.; Racko, J.; Rehacek, V.; Chymo, F.; Tapajna, M.; Harmatha, L. Silicon Based MIS Photoanode for Water Oxidation: A Comparison of RuO2 and Ni Schottky Contacts. *Appl. Surf. Sci.* **2018**, *461*, 48−53.
(34) McDowell, M. T.; Lichterman, M. F.; Carim, A. I.; Liu, R.; Hu, S.; Brunschwig, B. S.; Lewis, N. S. The Influence of Structure and Processing on the Behavior of TiO2 Protective Layers for Stabilization of N-Si/TiO2/Ni Photoanodes for Water Oxidation. *ACS Appl. Mater. Interfaces* **2015**, *7* (28), 15189−15199.
(35) Chen, Y. W.; Prange, J. D.; Dühnen, S.; Park, Y.; Gunji, M.; Chidsey, C. E. D.; McIntyre, P. C. Atomic Layer-Deposited Tunnel Oxide Stabilizes Silicon Photoanodes for Water Oxidation. *Nat. Mater.* **2011**, *10* (7), 539−544.
(36) Mei, B.; Pedersen, T.; Malacrida, P.; Bae, D.; Frydendal, R.; Hansen, O.; Vesborg, P. C. K.; Seger, B.; Chorkendorff, I. Crystalline TiO_2: A Generic and Effective Electron-Conducting Protection Layer for Photoanodes and -Cathodes. *J. Phys. Chem. C* **2015**, *119* (27), 15019−15027.
(37) Lichterman, M. F.; Sun, K.; Hu, S.; Zhou, X.; McDowell, M. T.; Shaner, M. R.; Richter, M. H.; Crumlin, E. J.; Carim, A. I.; Saadi, F. H.; et al. Protection of Inorganic Semiconductors for Sustained, Efficient Photoelectrochemical Water Oxidation. *Catal. Today* **2016**, *262*, 11−23.
(38) Scheuermann, A. G.; Lawrence, J. P.; Kemp, K. W.; Ito, T.; Walsh, A.; Chidsey, C. E. D.; Hurley, P. K.; McIntyre, P. C. Design Principles for Maximizing Photovoltage in Metal-Oxide-Protected Water-Splitting Photoanodes. *Nat. Mater.* **2016**, *15* (1), 99−105.
(39) Pan, L.; Kim, J. H.; Mayer, M. T.; Son, M.-K.; Ummadisingu, A.; Lee, J. S.; Hagfeldt, A.; Luo, J.; Grätzel, M. Boosting the Performance of Cu2O Photocathodes for Unassisted Solar Water Splitting Devices. *Nat. Catal.* **2018**, *1* (6), 412−420.
(40) Cai, Q.; Hong, W.; Jian, C.; Li, J.; Liu, W. Insulator Layer Engineering toward Stable Si Photoanode for Efficient Water Oxidation. *ACS Catal.* **2018**, *8* (10), 9238−9244.
(41) Hu, S.; Shaner, M. R.; Beardslee, J. A.; Lichterman, M.; Brunschwig, B. S.; Lewis, N. S. Amorphous TiO2 Coatings Stabilize Si, GaAs, and GaP Photoanodes for Efficient Water Oxidation. *Science* **2014**, *344* (6187), 1005−1009.
(42) Ji, L.; Hsu, H.-Y.; Li, X.; Huang, K.; Zhang, Y.; Lee, J. C.; Bard, A. J.; Yu, E. T. Localized Dielectric Breakdown and Antireflection Coating in Metal−Oxide−Semiconductor Photoelectrodes. *Nat. Mater.* **2017**, *16* (1), 127−131.
(43) Tilley, S. D. Recent Advances and Emerging Trends in Photo-Electrochemical Solar Energy Conversion. *Adv. Energy Mater.* **2019**, *9* (2), 1802877.
(44) Loget, G. Water Oxidation with Inhomogeneous Metal-Silicon Interfaces. *Curr. Opin. Colloid Interface Sci.* **2019**, *39*, 40−50.
(45) Zhu, W. J.; Ma, T.-P.; Tamagawa, T.; Kim, J.; Di, Y. Current Transport in Metal/Hafnium Oxide/Silicon Structure. *IEEE Electron Device Lett.* **2002**, *23* (2), 97−99.
(46) Wang, Y.; Yu, Z.; Zahid, F.; Liu, L.; Zhu, Y.; Wang, J.; Guo, H. Direct Tunneling through High- κ Amorphous HfO_2: Effects of Chemical Modification. *J. Appl. Phys.* **2014**, *116* (2), 023703.
(47) Eastment, R. M.; Mee, C. H. B. Work Function Measurements on (100), (110) and (111) Surfaces of Aluminium. *J. Phys. F: Met. Phys.* **1973**, *3* (9), 1738−1745.
(48) Eastman, D. E. Photoelectric Work Functions of Transition, Rare-Earth, and Noble Metals. *Phys. Rev. B* **1970**, *2* (1), 1−2.
(49) Mills, T. J.; Lin, F.; Boettcher, S. W. Theory and Simulations of Electrocatalyst-Coated Semiconductor Electrodes for Solar Water Splitting. *Phys. Rev. Lett.* **2014**, *112* (14), 148304.
(50) Sze, S. M.; Ng, K. K. *Physics of Semiconductor Devices*, 3rd ed.; Wiley-Interscience: Hoboken, NJ, 2007.
(51) Card, H. C.; Rhoderick, E. H. Studies of Tunnel MOS Diodes I. Interface Effects in Silicon Schottky Diodes. *J. Phys. D: Appl. Phys.* **1971**, *4* (10), 1589.

DOI: 10.1021/acsenergylett.9b01609
ACS Energy Lett. 2019, 4, 2632−2638